Long-Distance Coherent Propagation of High-Velocity Antiferromagnetic Spin Waves

Hanchen Wang, Rundong Yuan, Yongjian Zhou, Yuelin Zhang, Jilei Chen, Song Liu, Hao Jia, Dapeng Yu, Jean-Philippe Ansermet, Cheng Song, and Haiming Yu

Phys. Rev. Lett. **130**, 096701 — Published 28 February 2023
DOI: 10.1103/PhysRevLett.130.096701

Long-distance coherent propagation of high-velocity antiferromagnetic spin waves

Hanchen Wang,[1, 2, 3, *] Rundong Yuan,[1, *] Yongjian Zhou,[4, *] Yuelin Zhang,[1] Jilei Chen,[5, 2] Song Liu,[2, 5] Hao Jia,[2, 5] Dapeng Yu,[2, 5] Jean-Philippe Ansermet,[6, 5, †] Cheng Song,[4, ‡] and Haiming Yu[1, 2, §]

[1]*Fert Beijing Institute, MIIT Key Laboratory of Spintronics, School of Integrated Circuit Science and Engineering, Beihang University, Beijing 100191, China*
[2]*International Quantum Academy, Shenzhen 518048, China*
[3]*Department of Materials, ETH Zurich, Zurich 8093, Switzerland*
[4]*Key Laboratory of Advanced Materials (MOE), School of Materials Science and Engineering, Tsinghua University, Beijing 100084, China*
[5]*Shenzhen Institute for Quantum Science and Engineering, Southern University of Science and Technology, Shenzhen 518055, China*
[6]*Institute of Physics, Ecole Polytechnique Fédérale de Lausanne (EPFL), 1015, Lausanne, Switzerland*

(Dated: February 3, 2023)

We report on coherent propagation of antiferromagnetic (AFM) spin waves over a long distance (∼10 μm) at room temperature in a canted AFM α-Fe_2O_3 owing to the Dzyaloshinskii-Moriya interaction (DMI). Unprecedented high group velocities (up to 22.5 km/s) are characterized by microwave transmission using all-electrical spin wave spectroscopy. We derive analytically AFM spin-wave dispersion in the presence of the DMI which accounts for our experimental results. The AFM spin waves excited by nanometric coplanar waveguides have large wavevectors in the exchange regime and follow a quasi-linear dispersion relation. Fitting of experimental data with our theoretical model yields an AFM exchange stiffness length of 1.7 Å. Our results provide key insights on AFM spin dynamics and demonstrate high-speed functionality for AFM magnonics.

Spin waves or magnons [1–4] as collective spin excitations can transport coherent spin information in a magnetic media over long distances [5–7] without suffering from Ohmic loss, and are therefore promising for magnon-based computing with low-power consumption [8, 9]. So far, an overwhelming majority of magnonic research are conducted in ferro- or ferri-magnetic materials, such as yttrium iron garnet (YIG) [10–14], permalloy [15–18] and magnetic multilayers [19–21]. In ferromagnetic (FM) materials, long wavelength spin waves are predominantly affected by dipolar interactions, resulting in Damon-Eshbach (DE) and backward-volume (BV) modes with distinct configurations of the magnetization ($\mathbf{m}$) and wavevector ($\mathbf{k}$) and with non-degenerate dispersions [Fig. 1(a)]. This anisotropy hinders spin waves from propagating through a curved circuit [22] and leads to vulnerability to external field disturbances. Thus, it is desirable to excite high-k exchange spin waves in ferromagnets with short wavelengths that are substantially less anisotropic. Exchange spin waves in ferromagnets [23] follow a parabolic dispersion relation, suggesting an increasing group velocity for higher k. So far, it has been extremely challenging to excite exchange spin waves with a velocity around 1 km/s and a wavelength below 100 nm [6, 24, 25]. In antiferromagnetic (AFM) materials, these challenges and obstacles are inherently neutralized because spin waves are insensitive to disturbing magnetic fields [26] and can propagate with higher velocities [27]. However, new challenges arise as antiferromagnets have zero net moment [28]. In addition, antiferromagnetic spin waves fall typically in the THz or sub-THz frequency regime [29, 30] and are so far mostly excited using an optical method [27, 31] that is difficult to integrate with on-chip magnonic devices. Diffusive transport of multichromatic magnons have been studied by electrical injection and detection using Pt contacts [7, 32–36] which are insensitive to phase coherency. All-electrical excitation and detection of coherent AFM spin waves [37] are highly desired for magnonics, but remain challenging. Recently, advanced microwave technology based on solid-state extenders enabled frequency multiplication of conventional GHz source into sub-THz generators for all-electrical AFM magnon excitation [38, 39]. Until now, coherent AFM spin waves are electrically excited only with $k = 0$, i.e., antiferromagnetic resonance (AFMR) [31, 38–40] (e.g. black arrow in Fig. 1(b)), which has zero group velocity in a canted AFM [41]. High-velocity propagating AFM exchange spin waves with electrical excitation has not been realized so far.

In this Letter, we experimentally demonstrate coherent propagation of AFM exchange spin waves over a long distance (10 μm) in α-Fe_2O_3 with a high group velocity (22.5 km/s) at room temperature. The velocity is approximately one order of magnitude higher than that of FM exchange spin waves [6, 24, 25]. α-Fe_2O_3 also known as hematite is an insulating antiferromagnet [42–48] with ultra-low magnetic damping ($\sim 10^{-5}$) [32] and high Néel temperature (∼960 K) [49]. At room temperature (above its Morin temperature $T_M \simeq 260$ K), α-Fe_2O_3 is in an easy-plane antiferromagnetic phase, where its Néel vector $\mathbf{n}$ lies in the plane [Fig. 1(c)] normal to the corundum crystal c axis [50]. The bulk Dzyaloshinskii-Moriya interaction (DMI) in α-Fe_2O_3 induces a small canted moment [51] as shown in the inset of Fig. 1(b). The weak canted moment (∼1.2

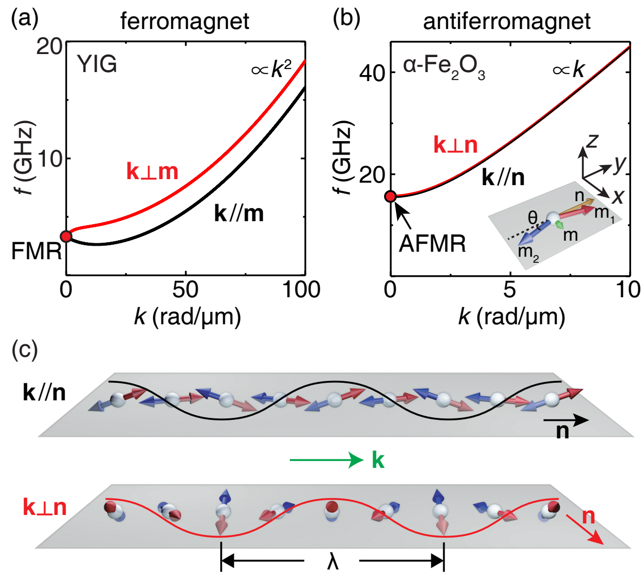

FIG. 1. (a) Ferromagnetic-type spin-wave dispersion for a 200 nm-thick YIG film. The $\mathbf{k} \perp \mathbf{m}$ and $\mathbf{k} \parallel \mathbf{m}$ modes are separated due to the dipolar interaction. The $k = 0$ mode is the ferromagnetic resonance (FMR). Exchange-dominated spin waves follow a quadratic k^2 relation. (b) Spin-wave dispersion of a canted antiferromagnet α-Fe_2O_3. The $\mathbf{k} \perp \mathbf{n}$ and $\mathbf{k} \parallel \mathbf{n}$ modes as illustrated in (c) are degenerate and adhere to a linear k dependence in exchange regime. The black arrow marks the antiferromagnetic resonance (AFMR) with $k = 0$. Inset illustrates the canting of two sublattices induced by the DMI. (c) Illustrations of exchange spin waves in an easy-plane antiferromagnet at two different configurations, namely, wavevector $\mathbf{k}$ parallel and perpendicular to Néel vector $\mathbf{n}$.

emu/cm^3) existing in the easy plane is characterized by x-ray diffraction and vibrating sample magnetometer as shown in Supplementary Material (SM) Fig. S1 [52]. Although the canted moment is negligibly weak as a net magnetic moment ($\sim$1% of YIG magnetic moment), it facilitates AFMR excitation with conventional microwave antennas [50, 51]. As the easy-plane anisotropy is remarkably small (H_a $\sim$0.06 mT), the AFMR frequency drops to around 20 GHz, which is accessible using conventional microwave techniques. The negligible easy-plane anisotropy also allows the Néel $\mathbf{n}$ to rotate freely in plane with respect to the spin-wave wavevector $\mathbf{k}$, as illustrated in Fig. 1(c) for $\mathbf{k} \parallel \mathbf{n}$ and $\mathbf{k} \perp \mathbf{n}$ as examples. Unlike in ferromagnets where $\mathbf{k} \perp \mathbf{m}$ (DE) and $\mathbf{k} \parallel \mathbf{m}$ (BV) behave differently [Fig. 1(b)], spin waves in antiferromagents are degenerate for $\mathbf{k} \perp \mathbf{n}$ and $\mathbf{k} \parallel \mathbf{n}$ [Fig. 1(c)] and any intermediate angle because the AFM spin-wave dispersion is not affected by dipolar interaction but fully determined by exchange interaction. Recently, Boventer *et al.* [51] have theoretically derived the AFMR ($k = 0$) formula for α-Fe_2O_3. However, literature on the spin-wave dispersion for an easy-plane antiferromagnet with DMI remains elusive.

Let us first derive and discuss the spin-wave dispersion for an antiferromagnet with DMI-induced canting and easy-plane anisotropy like that of α-Fe_2O_3 [Fig. 1(b)]. We consider a one-dimensional spin chain with two sublattices $\mathbf{m}_1$ and $\mathbf{m}_2$ that are antiferromagnetically coupled and confined in the easy plane. In the AFM system, the exchange energy, Zeeman energy, anisotropy energy and Dzyaloshinskii-Moriya (DM) energy constitute the total free energy, from which we obtain the equations of motion describing the dynamics of two spin sublattices in a mean-field approximation (see Sec. II in SM [52]),

$$\begin{cases} \dfrac{d\mathbf{m}_1}{dt} = -\gamma\mu_0\mathbf{m}_1 \times \left[\mathbf{H}_0 - H_\mathrm{ex}\mathbf{m}_2 - \dfrac{1}{2}H_\mathrm{ex}a_\mathrm{ex}^2\nabla^2\mathbf{m}_2 - H_\mathrm{A}\left(\mathbf{m}_1\cdot\hat{\mathbf{z}}\right)\hat{\mathbf{z}} + H_\mathrm{a}\left(\mathbf{m}_1\cdot\hat{\mathbf{y}}\right)\hat{\mathbf{y}} + H_\mathrm{DM}\left(\mathbf{m}_2\times\hat{\mathbf{z}}\right)\right] \\ \dfrac{d\mathbf{m}_2}{dt} = -\gamma\mu_0\mathbf{m}_2 \times \left[\mathbf{H}_0 - H_\mathrm{ex}\mathbf{m}_1 - \dfrac{1}{2}H_\mathrm{ex}a_\mathrm{ex}^2\nabla^2\mathbf{m}_1 - H_\mathrm{A}\left(\mathbf{m}_1\cdot\hat{\mathbf{z}}\right)\hat{\mathbf{z}} + H_\mathrm{a}\left(\mathbf{m}_2\cdot\hat{\mathbf{y}}\right)\hat{\mathbf{y}} - H_\mathrm{DM}\left(\mathbf{m}_1\times\hat{\mathbf{z}}\right)\right] \end{cases}, \quad (1)$$

where $\mathbf{H}_0$ is the external magnetic field, H_ex is the strength of the exchange field, a_ex is the exchange stiffness length (see SM Sec. II [52]), H_A (H_a) is the out-of-plane (in-plane) anisotropy and H_DM is the DM effective field. The exchange stiffness term consisting of H_ex and a_ex is discussed in the SM Table I [52] with a comparison between ferro-(ferri-)magnetic [55] and antiferromagnetic models [56]. Coordinate axes are defined in the inset of Fig. 1(b). Considering a small canting angle θ induced by the DMI, the cartesian coordinate defined with $\mathbf{n}$ and $\mathbf{m}$ at equilibrium is subsequently transformed to align with $\mathbf{m}_1$ or $\mathbf{m}_2$ in order to deduce the dynamics of the sublattices. By extracting the eigenfrequencies of Eq. 1, one derives the dispersion relations for both low-frequency and high-frequency AFM magnon modes (see SM Sec. II [52]). Since only the low-frequency one is relevant for our experiments, we present its spin-wave dispersion here as

$$f = \frac{\gamma\mu_0}{2\pi}\sqrt{H_0(H_0 + H_\mathrm{DM}) + 2H_\mathrm{a}H_\mathrm{ex} + H_\mathrm{ex}^2a_\mathrm{ex}^2k^2}, \quad (2)$$

where γ is the gyromagnetic ratio and μ_0 is the vacuum permeability. If on the one hand we take $k = 0$, the last term underneath the square root vanishes and thereby it reduces to the uniform AFMR of a canted

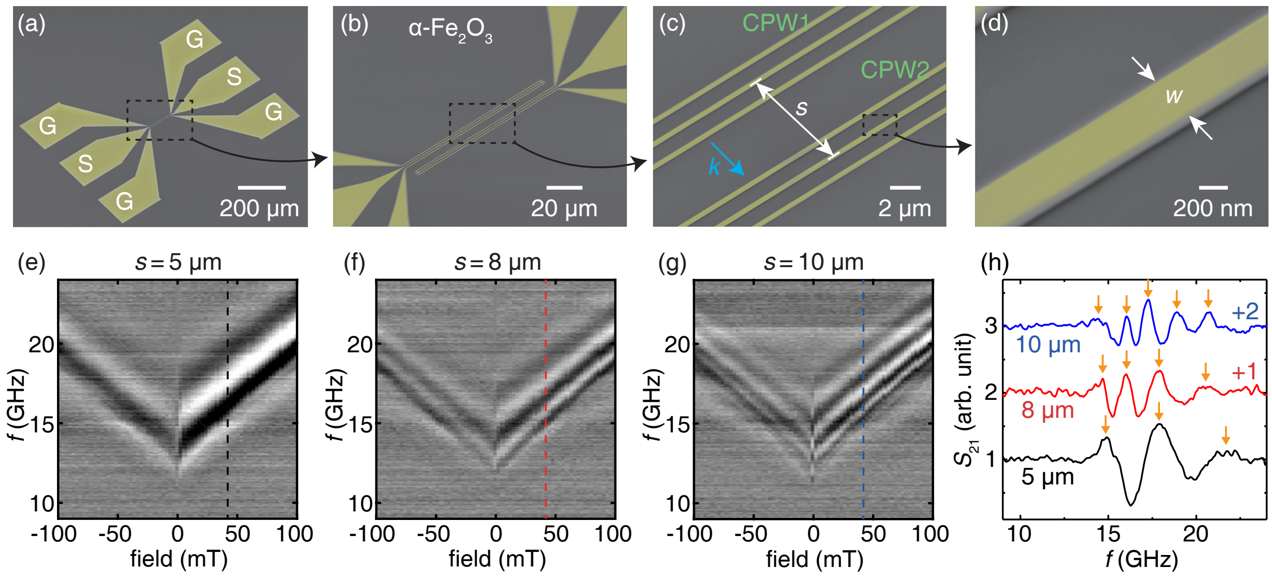

FIG. 2. (a) A global scanning electron microscopic (SEM) image of two coplanar waveguide (CPW) antennas integrated on α-Fe_2O_3 with a ground-signal-ground (GSG) design. The pitch of the contact pad is $250\,\mu$m, compatible with microwave probes. The gray background represents α-Fe_2O_3 substrate. (b) SEM image within the black dashed square area in (a). (c) SEM-resolved image of a CPW. The center-to-center distance s between CPW1 and CPW2 for this device is $8\,\mu$m. The blue arrow indicate the spin-wave wavevector k. The yellow-rendered parts are the gold conducting lines whose width $w = 380\,$nm is characterized by the further close-up image in (d). (e)-(g) Spin-wave transmission spectra S_{12} measured by a vector network analyzer (imaginary part of the S parameter) and plotted as a function of applied magnetic field for three devices with different propagation distances $s = 5, 8, 10\,\mu$m. (h) Lineplots extracted at 45 mT for propagation distances s. Spectra are shifted for clarity. Orange arrows highlight the peak positions.

antiferromagnet as studied by Boventer *et al.* [51]. If on the other hand we do not introduce the DMI in the system, the first term beneath the square root disappears and hence Eq. 2 becomes essentially the same as the dispersion for an easy-plane AFM such as NiO as analyzed by Rezende *et al.* [56] in the absence of DMI. In Fig. 1(b), we plot the spin-wave dispersion for the low-frequency mode in α-Fe_2O_3 based on Eq. 2 with $\mu_0 H_0 = 60$ mT. Here we take the exchange field $\mu_0 H_{\rm ex} = 1040$ T from Ref. [43]. By fitting the field-dependent AFMR in a flip-chip measurement ($k = 0$, see SM Fig. S7 [52]), we extract the effective DM field $\mu_0 H_{\rm DM} = 2.7$ T and $\mu_0 H_{\rm a} = 0.067$ mT. These values are close to those in Refs. [50, 51] and are adapted in plotting the dispersion in Fig. 1(b). Thus, the calculated dispersion relation predicts a group velocity of up to 26.5 km/s.

In the following, we present experimental demonstration of high-velocity propagation of spin waves in α-Fe_2O_3 with all-electrical excitation and detection. The DMI-induced small canted moment can couple with an external microwave field and therefore provides us an opportunity to excite antiferromagnetic spin waves with conventional coplanar waveguide antennas [6, 14–16, 25] fabricated on hematite using e-beam lithography and evaporation. Figures 2(a-d) show the scanning electron microscope (SEM) images of the measured device with a spin-wave propagation distance $s = 8\,\mu$m. Conventional coplanar waveguides (CPWs) with a ground-signal-ground (GSG) design are patterned on a 0.5 mm-thick α-Fe_2O_3 crystal with e-beam lithography and connected to a vector network analyzer (VNA) to excite and detect spin waves. The spin-wave wavevectors excited by the CPWs are along the $[11\bar{2}0]$ crystal orientation within the (0001) easy plane, which is the film plane. All measured devices are patterned on the same single-crystal film. Transmission spectra S_{21} (excitation at CPW1 and detection at CPW2) are measured by a VNA as a function of magnetic field, sweeping from negative to positive values. Data are shown in Figs. 2(e-g) for propagation distances (s) of $5\,\mu$m, $8\,\mu$m and $10\,\mu$m. The asymmetric amplitude of transmission spectra at positive and negative fields may arise from chiral magnetic near field emission induced by the nanoscale microwave antennas [57, 58] in combination with the unconventional time-reversal symmetry breaking of hematite, which is recently classified as an emergent magnetic phase altermagnetism [59]. A tentative theoretical model is discussed in SM Sec. II [52] taking into account of the chiral precession of the canted moment. Very recently, similar spin-wave non-reciprocity is reported in association with a surface mode observed in hematite [60]. Single spectra extracted at 45 mT are plotted together for three different propagation

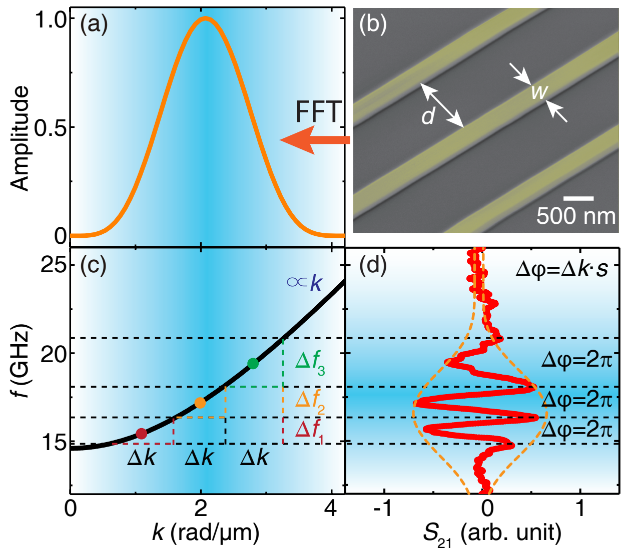

FIG. 3. (a) CPW-excited magnetic field wavevector distribution calculated by fast Fourier transformation (FFT) using the dimensions measured in the SEM image of (b) as w = 380 nm and d =1120 nm. (c) AFM spin-wave dispersion plotted for 51 mT, where the background intensity represents the wavevector distribution imposed by CPW as shown in (a). Three equivalent wavevector segments Δk project into different frequency spans Δf_1, Δf_2 and Δf_3 in accordance with the dispersion. The frequency spans manifests themselves as peak-to-peak separation in the measured transmission spectrum S_{21} in (d). These frequency spans correspond to a phase change of 2π after propagation over a certain distance s. The orange dashed curve in (d) defines effective excitation envelope corresponding to the wavevector distribution of CPW in (a). Horizontal and vertical black dashed lines are guide for the eyes.

distances in Fig. 2(h). The transmission signal amplitude decays due to spin-wave damping. With increasing s, the observed signal oscillation becomes denser and the number of peaks (marked by orange arrows) increases, for the following reason. The VNA is sensitive to the phase delay between both antennas and the interval between two adjacent peaks corresponds to a phase difference $\Delta\phi = 2\pi$. Over a certain propagation distance s, the phase change is given by $\Delta\phi = \Delta k \cdot s$, where Δk represents a broad wavevector excitation generated by the nanoscale CPW antennas, as shown in Fig. 3(a) and (b). When $\Delta\phi = \Delta k \cdot s$ reaches 2π, the second peak appears and the corresponding frequency interval Δf is observed [Fig. 3(d)]. Therefore, the spin-wave group velocity v_g can be estimated [14–16] using

$$v_\mathrm{g} = \frac{\partial\omega}{\partial k} \approx \frac{2\pi\Delta f}{\Delta k} = \frac{2\pi\Delta f}{2\pi/s} = \Delta f \cdot s. \quad (3)$$

At different parts of the spin-wave dispersion in Fig. 3(c), the frequency intervals Δf differ ($\Delta f_1 \neq \Delta f_2 \neq \Delta f_3$) in spite of an identical wavevector increment $\Delta k = 2\pi/s$. The higher-frequency part of the dispersion presents a steeper slope, $\Delta f_3 > \Delta f_2 > \Delta f_1$ as observed in Fig. 3(d). This indicates an increasing group velocity according to Eq. 3, given a fixed propagation distance s. Apart from the phase oscillation, the amplitude envelope (orange dashed arrows) is determined by the broad k excitation (blue shadow region) of the nanoscale CPW as characterized in Fig. 3(a). The frequency interval Δf_2 located at the center of the envelope around 17.5 GHz therefore exhibits the largest oscillation amplitude. Based on Eq. 3, we can extract the average group velocity at about 17.5 GHz (orange dot in Fig. 3(c)) from a linear fitting of the measured frequency interval Δf as a function of $1/s$, as shown in the bottom-right inset of Fig. 4. The slope of the fitted red line yields a group velocity of about 14.2 km/s. Following this method, we extract group velocities at different frequency bands and plot them in Fig. 4 as the red open squares. The data acquisition from linear fittings of Δf versus $1/s$ for frequencies of 15.9 GHz, 18.8 GHz and 20.7 GHz are presented in SM Sec. IV [52]. Two additional devices with slightly modified CPWs (Type 2 and Type 3) were also measured and group velocities obtained from these two samples (see SM Sec. IV [52]) are plotted as the orange circle and blue open triangle in Fig. 4. From the distance-dependent measurements, we extract a decay length of about 10 μm for coherent AFM spin waves (see SM Sec. V [52]). In conformity with the AFM spin-wave dispersion [Fig. 1(b)], we observe degenerate spin-wave modes (see SM Sec. VI [52]) for different angles (ϕ) between Néel vector ($\mathbf{n}$) and wavevector ($\mathbf{k}$), exhibiting almost identical spin-wave group velocities for different ϕ (top-left inset of Fig. 4).

The group velocities extracted from different samples (Fig. 4) increase asymptotically toward a saturated group velocity (linear range in dispersion) of $\gamma\mu_0 H_\mathrm{ex} a_\mathrm{ex}$. The group velocity as a function of frequency can be derived from the dispersion (Eq. 2). By fitting our data, we obtain an exchange stiffness length a_ex = 1.7 Å, which could also be considered as an effective lattice constant in the 1D spin-chain model. This value corresponds to an AFM exchange stiffness [61] of about 10 pJ/m and a saturated velocity [62] of 30.2 km/s (see SM Sec. II [52]). To approach the saturated velocity, we fabricate even smaller CPW antennas with larger wavevector k (∼5.2 rad/μm, see SM Sec. VII [52]). With these CPWs, we did not observe clear signal oscillations in transmission spectra, which we attribute to the impedance mismatch due to the down-scaling of the microwave antennas [63, 64]. For micrometer-scale CPW antennas with small wavevectors (∼1.0 rad/μm, see SM Sec. VII [52]), we again did not observe oscillating transmission signals owing to a low group velocity at the low-k limit.

In summary, we experimentally observed the coherent propagating AFM spin waves at room temperature

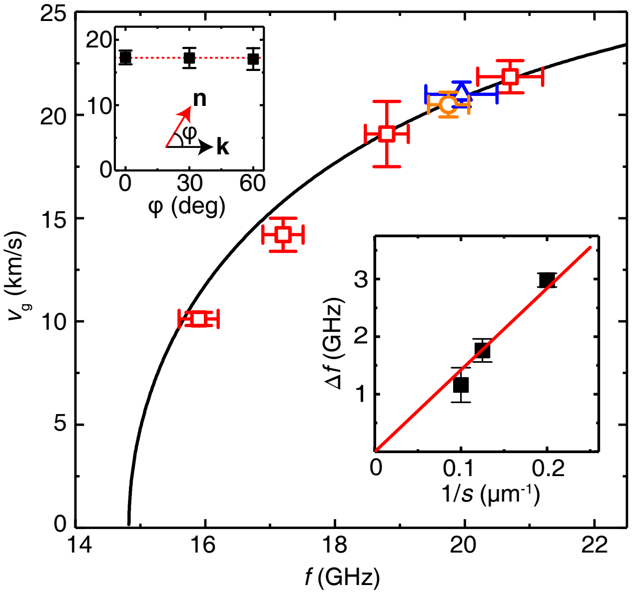

FIG. 4. AFM spin-wave group velocities for different frequencies extracted from the transmission spectra S_{21} at 51 mT. The values are given by the slope from a linear fit of Δf versus $1/s$ based on Eq. 3. Bottom-right inset shows an example for the linear fitting of the measurement data around 17.2 GHz for three different propagation distances $s = 5$ μm, 8 μm and 10 μm. Red open squares are data obtained from the samples with the CPW design shown in Fig. 3(b). Orange circles and blue open triangles are data obtained from the samples with two other CPW designs with slightly different dimensions as described in SM Sec. IV [52]. The solid line is the calculation taking the exchange length by fitting of our data $a_{\rm ex}$=1.7 Å. Top-left inset presents the angle dependent group velocities at 51 mT and around 18.8 GHz. The red dotted line is a horizontal line around 18 km/s.

in a single-crystal α-Fe_2O_3. Over a long distance of 10 μm, the coherence of AFM spin waves can still be detected with a high group velocity of up to 22.5 km/s. With measurements using CPW antennas of different propagation distances, the AFM spin-wave dispersion could be indirectly characterized via the relationship between group velocities and frequencies. These data could be accounted for with a theoretical model that takes into account exchange, DM, Zeeman and anisotropy energy. The AFM exchange stiffness length is estimated to be about 1.7 Å. One promising feature of AFM spin waves is their chirality, as it provides an additional degree of freedom. It has been shown that right- and left-handed modes can be detected electrically [39, 65]. High-velocity coherent propagating AFM spin waves is suggestive of great prospects for coherent AFM magnonics.

Note added.—During the revision of this manuscript, we become aware that recent reports on spin-wave dispersion of hematite studied by Brillouin light scattering [66] and non-reciprocial propagation of spin waves in hematite [60] have been posted.

The authors thank M. Elyasi, P. Gambardella, K. Yamamoto, and S. Maekawa for their helpful discussions. We wish to acknowledge the support by the National Key Research and Development Program of China Grant No. 2022YFA1402801 and 2022YFA1402603, NSF China under Grants No. 12074026, 52225106, 12241404 and U1801661, China Scholarship Council (CSC) under Grant No. 202206020091, and Shenzhen Institute for Quantum Science and Engineering, Southern University of Science and Technology (Grant No. SIQSE202007).

* These authors contributed equally to this work.
† jean-philippe.ansermet@epfl.ch
‡ songcheng@mail.tsinghua.edu.cn
§ haiming.yu@buaa.edu.cn

[1] V. Kruglyak, S. Demokritov, and D. Grundler, Magnonics. J. Phys. D Appl. Phys.**43**, 264001 (2010).
[2] A. V. Chumak, V. I. Vasyuchka, A. A. Serga, and B. Hillebrands, Magnon spintronics. Nat. Phys. **11**, 453-461 (2015).
[3] P. Pirro, V. I. Vasyuchka, A. A. Serga, and B. Hillebrands, Advances in coherent magnonics. Nat. Rev. Mater. **6**, 1114-1135 (2021).
[4] A. Barman *et al.*, The 2021 magnonics roadmap. J. Phys. Condens. Matter **33**, 413001 (2021).
[5] L. J. Cornelissen, J. Liu, R. A. Duine, J. B. Youssef, and B. J. van Wees, Long-distance transport of magnon spin information in a magnetic insulator at room temperature. Nat. Phys. **11**, 1022-1026 (2015).
[6] C. Liu, J. Chen, T. Liu, F. Heimbach, H. Yu, Y. Xiao, J. Hu, M. Liu, H. Chang, T. Stueckler *et al.*, Long-distance propagation of short-wavelength spin waves. Nat. Commun. **9**, 738 (2018).
[7] R. Lebrun, A. Ross, S. Bender, A. Qaiumzadeh, L. Baldrati, J. Cramer, A. Brataas, R. A. Duine, and M. Kläui, Tunable long-distance spin transport in a crystalline antiferromagnetic iron oxide. Nature **561**, 222-225 (2018).
[8] G. Csaba, A. Papp, and W. Porod, Perspectives of using spin waves for computing and signal processing. Phys. Lett. A **11**, 948-953 (2016).
[9] A. V. Chumak *et al.*, Advances in magnetics roadmap on spin-wave computing. IEEE Trans. Magn. **58**, 0800172 (2022).
[10] A. Serga, A. Chumak, and B. Hillebrands, YIG Magnonics. J. Phys. D: Appl. Phys. **43**, 264002 (2010).
[11] H. Chang, P. Li, W. Zhang, T. Liu, A. Hoffmann, L. Deng, and M. Wu, Nanometer-thick yttrium iron garnet films with extremely low damping. IEEE Magn. Lett. **5**, 6700 (2014).
[12] H. Qin, G. J. Both, S. J. Hämäläinen, L. Yao, and S. van Dijken, Low-loss YIG-based magnonic crystals with large tunable bandgaps. Nat. Commun. **9**, 5445 (2018).
[13] Q. Wang *et al.*, Spin pinning and spin-wave dispersion in nanoscopic ferromagnetic waveguides. Phys. Rev. Lett. **122**, 247202 (2019).

[14] H. Yu, O. Allivy Kelly, V. Cros, R. Bernard, P. Bortolotti, A. Anane, F. Brandl, R. Huber, I. Stasinopoulos, and D. Grundler, Magnetic thin-film insulator with ultra-low spin wave damping for coherent nanomagnonics. Sci. Rep. **4**, 6848 (2014).

[15] V. Vlaminck, and M. Bailleul, Current-induced spin-wave Doppler shift. Science **322**, 410 (2008).

[16] S. Neusser, G. Durr, H. G. Bauer, S. Tacchi, M. Madami, G. Woltersdorf, G. Gubbiotti, C. H. Back, and D. Grundler, Anisotropic propagation and damping of spin waves in a nanopatterned antidot lattice. Phys. Rev. Lett. **105**, 067208 (2010).

[17] A. Haldar, D. Kumar, and A. O. Adeyeye, A reconfigurable waveguide for energy-efficient transmission and local manipulation of information in a nanomagnetic device. Nat. Nanotechnol. **11**, 437-443 (2016).

[18] K. Wagner, A. Kákay, K. Schultheiss, A. Henschke, T. Sebastian, and H. Schultheiss, Magnetic domain walls as reconfigurable spin-wave nanochannels, Nat. Nanotechnol. **11**, 432-436 (2016).

[19] J. Han, P. Zhang, J. T. Hou, S. A. Siddiqui, and L. Liu, Mutual control of coherent spin waves and magnetic domain walls in a magnonic device. Science **366**, 1121-1125 (2019).

[20] M. Ishibashi, Y. Shiota, T. Li, S. Funada, T. Moriyama, and T. Ono, Switchable giant nonreciprocal frequency shift of propagating spin waves in synthetic antiferromagnets. Sci. Adv. **6**, eaaz6931 (2020).

[21] Y. Liu, Z. Xu, L. Liu, K. Zhang, Y. Meng, Y. Sun, P. Gao, H.-W. Zhao, Q. Niu, and J. Li, Switching magnon chirality in artificial ferrimagnet. Nat. Commun. **13**, 1264 (2022).

[22] K. Vogt, H. Schulheiss, S. Jain, J. E. Pearson, A. Hoffmann, S. D. Bader, and B. Hillebrands, Spin waves turning a corner. Appl. Phys. Lett. **101**, 042410 (2012).

[23] B. Kalinikos, and A. Slavin, Theory of dipole-exchange spin wave spectrum for ferromagnetic films with mixed exchange boundary conditions. J. Phys. C Solid State Phys. **19**, 7013 (1986).

[24] V. Sluka *et al.*, Emission and propagation of 1D and 2D spin waves with nanoscale wavelengths in anisotropic spin textures. Nat. Nanotechnol. **14**, 328-333 (2019).

[25] P. Che, K. Baumgaertl, A. Kúkolová, C. Dubs, and D. Grundler, Efficient wavelength conversion of exchange magnons below 100 nm by magnetic coplanar waveguides. Nat. Commun. **11**, 1445 (2020).

[26] V. Baltz, A. Manchon, M. Tsoi, T. Moriyama, T. Ono, and Y. Tserkovnyak, Antiferromagnetic spintronics. Rev. Mod. Phys. **90**, 015005 (2018).

[27] J. R. Hortensius, D. Afanasiev, M. Matthiesen, R. Leenders, R. Citro, A. V. Kimel, R. V. Mikhaylovskiy, B. A. Ivanov, and A. D. Caviglia, Coherent spin-wave transport in an antiferromagnet. Nat. Phys. **17**, 1001-1006 (2021).

[28] T. Jungwirth, X. Marti, P. Wadley, and J. Wunderlich, Antiferromagnetic spintronics. Nat. Nanotechnol. **11**, 231-241 (2016).

[29] O. Gomonay, V. Baltz, A. Brataas, and Y. Tserkovnyak, Antiferromagnetic spin textures and dynamics. Nat. Phys. **14**, 213-216 (2018).

[30] H. Qiu *et al.*, Manipulating Thz spin current dynamics by the Dzyaloshinskii-Moriya interaction in antiferromagnetic hematite. arXiv:2209.10175.

[31] T. Kampfrath, A. Sell, G. Klatt, A. Pashkin, S. Mährlein, T. Dekorsy, M. Wolf, M. Fiebig, A. Leitenstorfer, and R. Huber, Coherent terahertz control of antiferromagnetic spin waves. Nat. Photon. **5**, 31-34 (2011).

[32] R. Lebrun, A. Ross, O. Gomonay, V. Baltz, U. Ebels, A.-L. Barra, A. Qaiumzadeh, A. Brataas, J. Sinova, and M. Kläui, Long-distance spin-transport across the Morin phase transition up to room temperature in ultra-low damping single crystals of the antiferromagnet α-Fe_2O_3. Nat. Commun. **11**, 6332 (2020).

[33] A. Ross, R. Lebrun, O. Gomonay, D. A. Grave, A. Kay, L. Baldrati, S. Becker, A. Qaiumzadeh, C. Ulloa, G. Jakob, F. Kronast, J. Sinova, R. Duine, A. Brataas, A. Rothschild, and M. Kläui, Propagation length of antiferromagnetic magnons governed by domain configurations. Nano. Lett. **20**, 306-313 (2020).

[34] J. Han, P. Zhang, Z. Bi, Y. Fan, T. S. Safi, J. Xiang, J. Finley, L. Fu, R. Cheng, and L. Liu, Birefringence-like spin transport via linearly polarized antiferromagnetic magnons. Nat. Nanotechnol. **15**, 563-568 (2020).

[35] T. Wimmer, A. Kamra, J. Gückelhorn, M. Opel, S. Geprägs, R. Gross, H. Huebl, and M. Althammer, Observation of antiferromagnetic magnon pseudospin dynamics and the Hanle effect. Phys. Rev. Lett. **125**, 247204 (2020).

[36] S. Das, A. Ross, X. X. Ma, S. Becker, C. Schmitt, F. van Duijn, E. F. Galindez-Ruales, F. Fuhrmann, M.-A. Syskaki, U. Ebels, V. Baltz, A.-L. Barra, H. Y. Chen, G. Jakob, S. X. Cao, J. Sinova, O. Gomonay, R. Lebrun, and M. Kläui, Anisotropic long-range spin transport in canted antiferromagnetic orthoferrite $YFeO_3$. Nat. Commun. **13**, 6140 (2022).

[37] M. Dąbrowski, T. Nakano, D. M. Burn, A. Frisk, D. G. Newman, C. Klewe, Q. Li, M. Yang, P. Shafer, E. Arenholz, T. Hesjedal, G. van der Laan, Z. Q. Qiu, and R. J. Hicken, Coherent transfer of spin angular momentum by evanescent spin waves within antiferromagnetic NiO. Phys. Rev. Lett. **124**, 217201 (2020).

[38] C. Caspers, V. P. Gandhi, A. Magrez, E. de Rijk, and J.-Ph. Ansermet, Sub-terahertz spectroscopy of magnetic resonance in BiFeO3 using a vector network analyzer. Appl. Phys. Lett. **108**, 241109 (2016).

[39] J. Li *et al.*, Spin current from sub-terahertz-generated antiferromagnetic magnons. Nature **578**, 70-74 (2020).

[40] I. Boventer, H. Simensen, B. Brekke, M. Weides, A. Anane, M. Kläui, A. Brataas, and R. Lebrun, Antiferromagnetic cavity magnon polaritons in collinear and canted phases of hematite. Phys. Rev. Appl. (to be published) arXiv:2203.10924.

[41] S. Rezende, A. Azevedo, and R. L. Rodríguez-Suárez, Introduction to antiferromagnetic magnons. J. Appl. Phys. **126**, 151101 (2019).

[42] F. J. Morin, Electrical properties of α-Fe_2O_3 containing titanium. Phys. Rev. **83**, 1005 (1951).

[43] P. J. Besser, A. H. Morrish, and C. W. Searle, Magnetocrystalline anisotropy of pure and doped hematite. Phys. Rev. **153**, 632 (1967).

[44] H. Jani, J.-C. Lin, J. Chen, J. Harrison, F. Maccherozzi, J. Schad, S. Prakash, C.-B. Eom, A. Ariando, T. Venkatesan, and P. G. Radaelli, Antiferromagnetic half-skyrmions and bimerons at room temperature. Nature **590**, 74-79 (2021).

[45] F. P. Chmiel *et al.*, Observation of magnetic vortex pairs at room temperature in a planar α-Fe_2O_3/Co

heterostructure. Nat. Mater. **17**, 581-585 (2018).

[46] A. Wittmann *et al.*, Role of substrate clamping on anisotropy and domain structure in the canted antiferromagnet α-Fe_2O_3. Phys. Rev. B **106**, 224419 (2022)

[47] F. J. dos Santos, M. dos Santos Dias, and S. Lounis, Modeling spin waves in noncollinear antiferromagnets: Spin-flop states, spin spirals, skyrmions, and antiskyrmions. Phys. Rev. B **102**, 104436 (2020).

[48] P. X. Zhang, C.-T. Chou, H. Yun, B. C. McGoldrick, J. T. Hou, K. A. Mkhoyan, L. Liu, Control of Néel vector with spin-orbit torques in an antiferromagnetic insulator with tilted easy plane. Phys. Rev. Lett. **129**, 017203 (2022).

[49] M. Białek, J. Zhang, H. Yu, and J.-Ph. Ansermet, Antiferromagnetic resonance in α-Fe_2O_3 up to its Néel temperature. Appl. Phys. Lett. **121**, 032401 (2022).

[50] H. Wang, Y. Xiao, M. Guo, E. Lee-Wong, G. Q. Yan, R. Cheng, and C. R. Du, Spin pumping of an easy-plane antiferromagnet enhanced by Dzyaloshinskii–Moriya interaction. Phys. Rev. Lett. **127**, 117202 (2021).

[51] I. Boventer, H. T. Simensen, A. Anane, M. Kläui, A. Brataas, and R. Lebrun, Room-temperature antiferromagnetic resonance and inverse spin-Hall voltage in canted antiferromagnets. Phys. Rev. Lett. **126**, 187201 (2021).

[52] See Supplementary Material for single-crystal α-Fe_2O_3 sample characterizations, spin-chain model for easy-plane antiferromagnetic spin waves with Dzyaloshinskii-Moriya interaction, magnetic parameters extracted from the field-dependent reflection spectra, different types of CPW antennas and their AFM spin-wave transmission spectra, group velocities extracted from experimental results, decay length estimated by experimental results, propagating AFM spin-wave transmission measurements at different angles between wavevector **k** and Néel vector **n**, spin-wave transmission spectra measured on the CPW antennas with higher and lower wavevectors, which includes Refs. [53, 54].

[53] J.-Ph. Ansermet, and S. D. Brechet, *Principles of thermodynamics.* (Cambridge University Press, 2019).

[54] R. M. Cornell, and U. Schwertmann, *The Iron Oxides: Structure, Properties, Reactions, Occurrences, and Uses.* (Wiley-vch Weinheim, 2003), Chap. 2.

[55] E. H. Turner, Interaction of phonons and spin waves in yttrium iron garnet. Phys. Rev. Lett. **5**, 100 (1960).

[56] S. M. Rezende, R. L. Rodríguez-Suárez, and A. Azevedo, Diffusive magnonic spin transport in antiferromagnetic insulators. Phys. Rev. B **93**, 054412 (2016).

[57] T. Yu, and G. E. W. Bauer, Noncontact spin pumping by microwave evanescent fields. Phys. Rev. Lett. **124**, 236801 (2020).

[58] V. E. Demidov, M. P. Kostylev, K. Rott, P. Krzysteczko, G. Reiss, and S. O. Demokritov, Excitation of microwaveguide modes by a stripe antenna. Appl. Phys. Lett. **95**, 112509 (2009).

[59] L. Smejkal, J. Sinova, and T. Jungwirth, Emerging Research Landscape of Altermagnetism. Phys. Rev. X **12**, 040501 (2022).

[60] A. El Kanj, O. Gomonay, I. Boventer, P. Bortolotti, V. Cros, A. Anane, and R. Lebrun, Evidence of non-degenerated, non-reciprocal and ultra-fast spin-waves in the canted antiferromagnet α-Fe_2O_3. arXiv:2301.06329.

[61] A. Šcholl, M. Liberati, E. Arenholz, H. Ohldag, and J. Stöhr, Creation of an antiferromagnetic exchange spring. Phys. Rev. Lett. **92**, 247201 (2004).

[62] E. J. Samuelsen, and G. Shirane, Inelastic neutron scattering investigation of spin waves and magnetic interactions in α-Fe_2O_3. Phys. Stat. Sol. **42**, 241-256 (1970).

[63] F. Ciubotaru, T. Devolder, M. Manfrini, C. Adelmann, and I. Radu, All electrical propagating spin wave spectroscopy with broadband wavevector capability. Appl. Phys. Lett. **109**, 012403 (2016).

[64] J. Lucassen, C. F. Schippers, L. Rutten, R. A. Duine, H. J. Swagten, B. Koopmans, and R. Lavrijsen, Optimizing propagating spin wave spectroscopy. Appl. Phys. Lett. **115**, 012403 (2019).

[65] Y. Liu, H. Liu, W. Yuan, Y. Li, J. Li, Q. Shao, R. Cheng, and J. Shi, Controlling antiferromagnetic magnon polarization by interfacial exchange interaction. Phys. Rev. Appl. **18**, 034005 (2022).

[66] M. Hamdi, F. Posva, and D. Grundler, Spin wave dispersion of ultra-low damping hematite (α-Fe_2O_3) at GHz frequencies. arXiv:2212.11887.